X-643-64-50

TM X-55013

33P

SOLAR CYCLE CHANGES IN INNER ZONE PROTONS

MARCH 1964

NASA — GODDARD SPACE FLIGHT CENTER

GREENBELT, MARYLAND

ABSTRACT

27250

Time dependent calculations of the inner Van Allen belt proton population show that large changes of the population up to a factor of 50 will take place during the solar cycle. The effect is most pronounced for the region of B-L space corresponding to minimum altitudes of 300-700 km. Because different energy protons respond to the changing solar cycle at different rates the proton energy spectra will change with time also.

Author

Solar Cycle Changes in Inner Zone Protons

Robert C. Blanchard†
and
Wilmot N. Hess

The purpose of this paper is to calculate the expected changes in inner zone proton populations with time in the solar cycle.

Freden and White [1959] identified the penetrating component of the inner zone of the Van Allen belt as due to energetic protons and measured the energy spectrum of the protons of $E > 75$ Mev. This and subsequent experimental work on Atlas rockets [Freden and White, 1960; Freden and White, 1962; Armstrong, Harrison, Heckman and Rosen, 1961] has confirmed and extended this finding and we now have a well-established proton energy spectrum at $L \sim 1.4$, $B \sim .20$, which is about apogee for these flights, for near solar maximum (see Fig. 1). The analysis of this spectrum [Freden and White, 1960] has shown conclusively that the protons are produced by neutron decay.

One of the features of this component of the radiation belt is the time constancy. Measurements after a solar flare [Freden and White, 1962] gave essentially the same fluxes of protons as before the flare. For $L > 1.6$ changes in proton spectra are seen [Naugle and Kniffen, 1961] associated with solar proton events [Pizzella, 1961]. These may be explainable in terms of neutrons produced in the polar regions by solar protons [Lenchek, 1962; Lingenfelter, to be published]. For $L < 1.6$ only gradual changes in the proton populations have been observed on Explorer VII [Pizzella, 1961].

---

† Done as part of the requirements for a Master's Degree from the College of William and Mary.

It was originally suggested [Pizzella, 1961] that such changes implied that neutrons could not produce all inner zone protons but this does not seem to be the case. Hess [1962] showed that slow changes in proton population were expected due to changes in the galactic cosmic ray flux during the solar cycle and more importantly due to changes in the upper atmospheric density during the solar cycle. We will now make a quantitative discussion of the expected changes in proton populations for $L < 1.6$.

The continuity equation for protons is usually written [Singer, 1958; Hess, 1959; Freden and White, 1960]

$$\frac{dN(E)}{dt} = + S(E) - L(E) + \frac{d}{dE}\left[N(E) \frac{dE}{dx} v \right] = 0 \qquad (1)$$

and the steady state population of protons $N(E)$ solved for. We are now interested in time variations so we will write the time dependent form of this equation

$$\frac{dN(E,t)}{dt} = + S(E,t) - L(E,t) + \frac{d}{dE}\left[N(E,t) \frac{dE}{dx}(t) v \right] \qquad (2)$$

The source term $S(E,t)$ will use the neutron decay source strength of Hess for solar maximum $S(E)$ multiplied by a function of time $f(t)$ to consider the solar cycle variation in galactic cosmic ray flux as determined by McDonald and Webber [1961]

$$S(E\ t) = S(E)\ f(t) = \frac{0.8\ E^{-2.0}}{\upsilon\gamma T_n} \quad \frac{r_e^3}{r}\ F(t) \tag{3}$$

where $f(t)$ varies from 1.0 at solar max to 1.25 at solar min in a similar way to Fig. 2.

For the loss term $L(E,t)$ following Freden and White [1960] we consider nuclear collisions

$$L(E,t) = N(E,t)\ v \sum_I \sigma_i\ \bar{\rho}_i\ (t) \tag{4}$$

where $\bar{\rho}_i(t)$ is the average atmospheric density of atmospheric component i (O_2, O, N_2 or He) and σ_i is the inelastic cross section for collisions (assumed geometric).

The last term in equation 2, the change in proton population due to slowing down, varies with the solar cycle due to the atmospheric density change

$$\frac{dE}{dx} = \left[\frac{\bar{\bar{\rho}}\ (t)}{2.69 \times 10^{19}}\right] \times \left.\frac{dE}{dx}\right|_{NTP} \tag{5}$$

where $\bar{\bar{\rho}}\ (t)$ is the average atmospheric density of equivalent oxygen atoms. The variation of $\bar{\rho}_i(t)$ and $\bar{\bar{\rho}}\ (t)$ with time in the solar cycle is the major reason for the change in proton population.

Average Atmospheric Densities

A major part of this problem was to determine the average atmospheric densities used in calculating the loss rate of trapped protons by coulomb scattering. To do this the theoretical model of the upper atmosphere developed by Harris and Priester [1962] was used. This model gives the time dependences of the atmosphere for both solar cycle and diurnal variations. It agrees well with several measurements of density by satellite drag (King-Hele, 1963; Bryant, to be published) and recently has been checked by preliminary data of densities from the Explorer XVII satellite./ Spencer et al [1963] This model atmosphere is the most complete description of the time dependence of atmospheric densities available and agrees well with the current experimental data. We must perform several operations on the H and P model data to get it in form to use for this problem. Harris and Priester give the atom densities n_i of the several atmospheric constituents i in the form of,

$$n_i\ (h,\ t,\ S)$$

where h is altitude above the earth, t is local time, and S is a model parameter related to, but not the same as, the intensity of the average 10 cm solar flux, $\bar{F}$, in watts/m^2-cps x 10^{-22}. Recent studies of atmospheric densities [Harris and Priester, 1963] show that the model number S is the same as $\bar{F}$ near solar max but near solar min $S < \bar{F}$. For example,

$\bar{F} = 70$ corresponds to the model $S = 100$. Fig. 2 shows the solar cycle variation of S we have used based on the last solar cycle.

The first operation on the H and P atmosphere is to average over local time. The protons we will consider live long enough so that they will encounter the midday density bulge and the nighttime minimum many times and will average them out.

Secondly, we perform a longitude average. As the particles drift around the earth their mirror points do not stay at constant altitude but rather follow a certain path in B-L space. Several such constant B-L rings are shown in altitude-longitude coordinates in Fig. 3. The particles dip lowest in the South Atlantic due to the nature of the earth's magnetic field. A B-L map of minimum altitudes is shown in Fig. 4. Due to the variation in altitude of the protons' mirror point, longitude averages were made using the B-L rings every ten degrees in both northern and southern hemispheres. This step gives the average mirror point density for a proton's motion. Walt has recently shown that the protons do not drift in longitude at a constant rate because of the variation of the magnetic field gradient and field line curvature. This effect is ignored here. It probably amounts to about a 20 percent correction on average densities. Values of atmospheric densities are not known that well now anyway.

The third operation on the H and P atmosphere is to average over a bounce from one mirror point to the conjugate mirror point. Since the protons live much longer than a bounce period, and since no change in direction of the proton is considered during slowing, it is permissible to average the density in this fashion. A dipole field is assumed in carrying out this step.

Ray [1960] gave the bounce averaging process as

$$\rho = \frac{\int \rho(\lambda) ds}{\int ds} \tag{6}$$

where the element of length along the particle's orbit is

$$ds = \frac{v dt}{\cos \alpha} = \frac{d\ell}{\cos \alpha} \tag{7}$$

where $d\ell$ is the element of length along the field line. Using

$$d\ell^2 = dr^2 + r^2 d\lambda^2 \tag{8}$$

and

$$r = L \cos^2 \lambda \tag{9}$$

with the mirror equation and the expression for the magnetic field variation along a field line

combining and substituting in equation 6 gives

$$\overline{\rho}_i = \frac{\int \rho_i(\lambda) A(\lambda) d\lambda}{\int A(\lambda) d\lambda} \tag{10}$$

where

$$A(\lambda) = \frac{\cos^4 \lambda \sqrt{1 + 3 \sin^2 \lambda}}{\left[\cos^6 \lambda \, (1 + 3 \sin^2 \lambda_m)^{\frac{1}{2}} - \cos^6 \lambda_m \, (1 + 3 \sin^2 \lambda)^{\frac{1}{2}} \right]^{\frac{1}{2}}} \qquad (11)$$

The subscript m here corresponds to the particles' mirror point. This bounce averaged density has been integrated on a computer.

The last step is to combine the five i constituents N_2, O_2, O, He and H to give the averaged number of equivalent oxygen atoms

$$8 \bar{\bar{\rho}} = 14 \bar{\rho} (N_2) + \bar{\rho} (O) + 16 \bar{\rho} (O_2) + 2 \bar{\rho} (He) + \bar{\rho} (H) \qquad (12)$$

Values of $\bar{\bar{\rho}}$ at different times in the solar cycle for L = 1.25 are shown in Figure 5.

We can use the data on the rate of energy loss dE/dx for oxygen at NTP [Aaron, Hoffman and Williams, 1949] in equation 5 with this averaged density $\bar{\bar{\rho}}$ to calculate the loss rate.

RESULTS

Equation (2) is integrated stepwise starting with $N(E) = 0$ at $t = 0$ to build up to an oscillating proton population which is the same from one solar cycle to the next. In Figure 6 is shown the number of solar cycles after which the population change per cycle is less than 1% for $L = 1.25$. After achieving this final condition the proton energy spectrum varies during one solar cycle as shown in Figures 7-11. The dotted curves top and bottom in these figures are what the proton spectrum would be if steady state conditions were achieved at solar max and solar min. Steady state clearly is not achieved for high energy protons or for high altitudes.

It is also interesting that this calculation predicts a spectral peak above 100 Mev for certain conditions (Figure 7, year 3) due to the time lag in different energy protons adjusting to solar cycle changes.

Figures 12 and 13 show time histories for various conditions. Large variations from solar max to solar min populations are seen in these figures. The amplitude of these changes for $L = 1.25$ and 1.40 are shown in Figures 14 and 15.

A comparison of past experimental results and the calculations of this paper is shown in Table I. In discussing these experiments we can consider three types of information.

In comparing time changes of the proton fluxes two situations occur:

1. Some individual experiments run long enough (a year or more) so that they should see proton flux changes directly. From Table I,

experiments (c) and (d) are of this time. Although in experiment (d) it is not one experiment on one satellite, it is many identical experiments on essentially identical satellites, and therefore this experiment falls in this category.

2. Different experiments on different satellites can be compared to provide data on proton flux changes. Data of this type is given in experiments (a), (e) and (f) in Table I.

The third type of data is given by:

3. Direct measurement of the proton energy spectrum in one experiment. Experiments (a), (b), (e), (f) and (g) are of this type.

In comparing flux time change experiments of type (1) with the calculations, the agreement is good. Two experiments covering the period 1959 to 1962 give results consistent with the calculations.

Comparing with type (2) data does not work as well. The observed changes of flux with time agree qualitatively than those predicted but not quantitatively. The experimental flux ratios are smaller than the calculated ones. Two remarks are in order here. First, type (2) data usually has larger errors attached to it than type (1) because it involves the systematic errors of two experiments while type (1) data involves no systematic errors--only statistical errors are involved in the time variations in the flux. Because of this the experimental flux ratios using type (2) data are probably not as accurate as those using type (1)

data. Secondly all the comparisons of type (2) data involve Explorer IV data; so there is no independent check of experimental consistency.

We may have over-estimated the amplitude of the change of proton populations in this present calculation by as much as a factor of two because our solar cycle model uses S = 70 at solar minimum while recent data of Harris and Priester (1963) shows that S = 100 is probably more appropriate. Changing the shape of the model solar cycle (Figure 2) will also affect the results of the calculation. The solar cycle must rise more rapidly towards solar max. than it falls to solar min. in order to produce the changes in spectrum calculated here. Solar cycle 16 was quite symmetrical and should not give the calculated results.

Of the five experiments of type (3) that help understand the proton energy spectrum the first two (a) and (b) in 1960 showed a modest sized peak at about E ≈ 40 Mev. The more recent experiment (g) of Rowland et al in 1962 shown in Figure 16 does not show such a peak. The solid curve on Figure 16 compared with the data of Rowland is the results of the present calculations normalized. The agreement is fairly good. Recent experiments (f)(g) show a large low energy proton population but cannot be compared with early experiments because the early ones did not go down to such low energies. Figures 7-11 show that the calculated spectral shape should not change much during the period of these measurements--from 6 to 9 years solar cycle time. The proton fluxes should increase but the shape of the spectrum stays nearly the same. Striking changes in spectral shape should occur on the upswing of the solar cycle. The agreement with spectral shape in Figure 16 is not bad but the peaks in experiments (a) and (b) should not occur at t = 6. It may be that a neutron absorption as suggested by Freden and White (1962) is required to explain the peak.

All of the information presented so far on Figures 6 through 15 are mirror point fluxes M, that is, the flux of protons mirroring per unit volume at one particular B and L. For low altitudes where the atmosphere changes rapidly with altitude it is nearly correct to compare this flux with measured omnidirectional flux values. For these low altitudes the omnidirectional flux is very nearly the same as the mirror point flux. To show a more complete picture of the solar cycle proton changes we have converted to omnidirectional fluxes using equations (24) of Hess and Killeen (1961). Figure 17 shows a calculated R-λ map of the 25 Mev proton omnidirectional fluxes J at solar max and solar min. An isoflux contour is clearly at lower R for solar minimum.

In conclusion we have shown that large changes in proton fluxes will take place during the solar cycle for those regions of B-L space corresponding roughly to minimum altitudes of about 300-700 km. Changes in proton spectra will occur also. Comparison of the calculations with available experimental information are not conclusive. Some kinds of experimental data agree quantitatively with the calculations. Other data agrees qualitatively but not quantitatively. The crucial tests of the calculations will involve measuring changes in the proton flux and spectrum as we approach solar maximum during 1966-68. We know experimentally (King-Hele 1963) that the atmospheric density changes used in the calculation are reasonable. These calculated effects must take place with about the magnitudes shown here unless there are features of the inner belt protons which we do not now understand.

REFERENCES

1. Armstrong, A. H., F. B. Harrison, H. H. Heckman, and L. Rosen, Charged particles in the inner Van Allen radiation belt, J. Geophys. Research, 66 351-8 (1961)

2. Aron, W. A., B. S. Hoffman, F. C. Williams, "Range-Energy Curves" (2nd Rev. 1949) U. S. A.E.C., Univ. of Calif. Rad. Lab.

3. Bryant, R., Densitites Obtained from Drag on the Explorer XVII Satellite, to be published.

4. Filz, R., and H. Yagoda "Observations on Trapped Protons in Emulsions Recovered from Satellite Orbits" to be published in Space Research IV and private communication.

5. Freden, S. C., R. S. White, Protons in the Earth's Magnetic Field Phys. Rev. Letters 3 9-11 (1959).

6. Freden, S. C., R. S. White, "Particle Fluxes in the Inner Radiation Belt" J. of Geophys. Res., vol. 65, no. 5, May, 1960.

7. Freden, S. C., R. S. White, "Trapped Proton and Cosmic-Ray Albedo Neutron Fluxes", J. of Geophys. Res., vol. 67, no. 1, January 1962, p. 25.

8. Freden, S. C., and G. A. Paulikas, "Trapped Protons at Low Altitudes in the South Atlantic Magnetic Anomoly" Tech. Doc. SSD-TDR-63-342 Aerospace Corporation, Inglewood, Calif.

9. Harris, I., and W. Priester, "Theoretical Models for the Solar-Cycle Variation of the Upper Atmosphere" X-640-62-70, June, 1962, and J. A. S. 19 286 (1962), Time-Dependent Structure of the Upper Atmosphere.

10. Harris, I., and W. Priester, Relation between Theoretical and Observational Models of the Upper Atmosphere, J. of Geophysical Res. 68 5891, 1963.

11. Heckman, H. and G. H. Nakano "East-West Assymmetry in the Flux of Mirroring Geomagnetically Trapped Protons" J.G.R. 68 2117, 1963 and private communications.

12. Hess, W. N., "Discussion of paper by Pizzella, McIlwain and Van Allen" J. of Geophys. Res., 67 4886 (1962) and "Lifetime and Time Histories of Trapped Radiation Belt Particles" Space Research Vol. III, to be published.

13. Hess, W. N. and J. Killeen "Spacial Distribution of Electrons from Neutron Decay in the Outer Radiation Belt" J. G. R. 66 3671 (1961).

14. Hess, W. N., "Van Allen Belt Protons from Cosmic-Ray Neutron Leakage" Phys. Rev. Letter 3 11 (1959).

15. King-Hele, D. G., "Decrease in Upper-Atmosphere Density since the Sunspot Maximum of 1957-58" Nature 198 832 (1963).

16. Rowland, J. H., J. C. Bakke, W. L. Imhof, and R. V. Smith, "Radiation Environment Experiment" Tech. Report SSD-TDR-63-194, Lockheed Missiles and Space Co., Palo Alto, California.

17. Lencheck, A. M., J. of Geophys. Res., 67 2145 (1962).

18. Lingenfelter, R. E., to be published.

19. McDonald, F. B., and W. R. Webber, "A study of the rigidity and charge dependence of primary cosmic ray temporal variations" Journal of the Physical Society of Japan, vol. 17, Supplement A-II, Proceedings of the International Conference on Cosmic Rays and the Earth Storm, September 4-15, 1961.

20. Naugle, J. E., and D. A. Kniffen, Flux and Energy Spectra of the Protons in the Inner Van Allen Belt, Phys. Rev. Letter 7 3 (1961) and "Variations of the Proton Energy Spectrum with Position in the Inner Van Allen Belt" J.G.R. 68 4065 (1963).

21. Pizzella, G., C. E. McIlwain and J. A. Van Allen, Time Variations of Intensity of the Earth's Inner Radiation Zone, October 1959 through December 1960, J.G.R. 67 1235 1962.

22. Ray, Ernest C., "On the Theory of Protons Trapped in the Earth's Magnetic Field" J. of Geophys. Res., vol. 67, no. 4, April 1960, pp. 1125-1133.

23. Singer, S. F., "Trapped Albedo Theory of the Radiation Belt" Phys. Rev. Letter 1 181 (1958).

24. Spencer, N. W., L. H. Brace, C. R. Corignan, D. R. Taeusch and H. Niemann, "The Concentration and Temperature of Molecular Nitrogen and Electrons in the 120 to 350 km Region", L. H. Brace and N. W. Spencer, "Geophysical Implications of Explorer XVII Electrostatic Probe Measurements", Horowitz, R., and G. P. Newton, "First Direct In-Site Measurements of Atmospheric Density from Explorer XVII", Reber, C. C., "Preliminary Results Regarding Neutral Atmosphere Composition from the Explorer XVII Satellite", abstracts at the Boulder AGU Meeting, Dec. 1963, Transactions of AGU 44 884 (1963).

FIGURE CAPTIONS

1. The experimentally measured inner zone proton energy spectrum (Freden and White 1962) for $L \sim 1.4$ $B \sim .20$.

2. Solar cycle used in these calculations S is the Harris and Priester (1962) model parameter which is related to but not the same as the 10 cm flux intensity.

3. Variation of the altitude of B-L rings with longitude.

4. B-L map of minimum altitudes.

5. Average atmospheric densities at different times of the solar cycle at different B-L points.

6. The number of solar cycles needed for a group of protons to come within 1% of its final oscillating population for $L = 1.25$ starting with $N(E) = 0$ at $t = 0$.

7. Proton Energy Spectra at different times in the solar cycle for $L = 1.40$, $B = .225$. The curves are labeled by the time in years from solar min.

8. Proton Energy Spectra at different times in the solar cycle for $L = 1.40$, $B = .201$. The curves are labeled by the time in years from solar min.

9. Proton Energy Spectra at different times in the solar cycle for $L = 1.40$, $B = .181$. The curves are labeled by the time in years from solar min.

10. Proton Energy Spectra at different times in the solar cycle for $L = 1.25$, $B = .207$. The curves are labeled by the time in years from solar min.

11. Proton Energy Spectra at different times in the solar cycle for $L = 1.25$, $B = .183$. The curves are labeled by the time in years from solar min.

12. Proton time histories for $L = 1.40$, $B = .225$.

13. Proton time histories for $L = 1.40$, $B = .201$.

14. The amplitude of the proton population change during the solar cycle for $L = 1.25$.

15. The amplitude of the proton population change during the solar cycle for $L = 1.4$ and 1.6.

16. The energy spectrum of inner zone protons measured by Rowland et. al. 1963 on an Atlas pod at $L = 1.27$, $B = .216$ shown for comparison is the spectrum calculated in this paper for $L = 1.27$, $B = .207$, $t = 9$.

17. An R-λ map of the omnidirectional flux of $E = 25$ Mev protons at solar max and solar min.

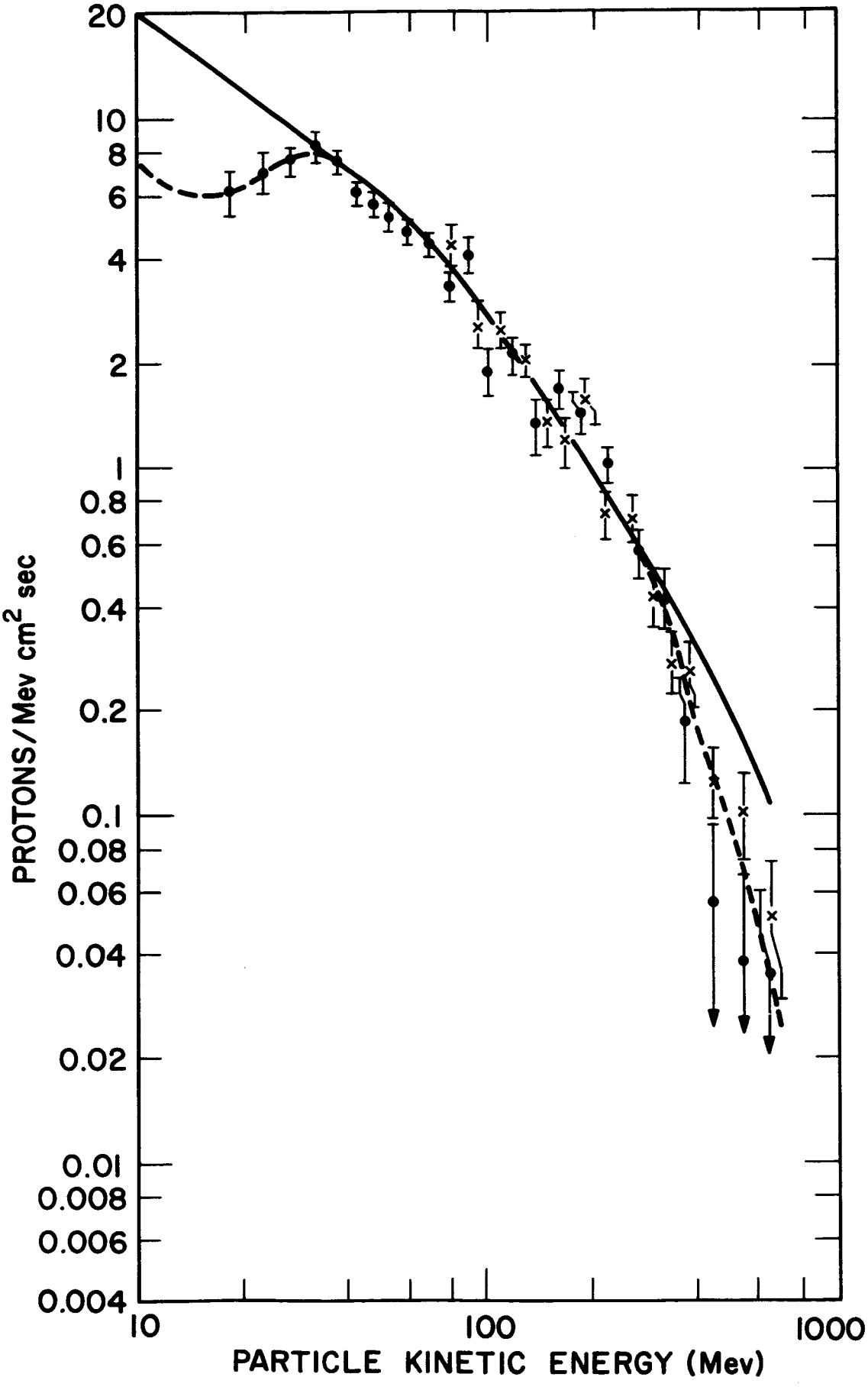
20
10
8
6
4
2
1
0.8
0.6
0.4
0.2
0.1
0.08
0.06
0.04
0.02
0.01
0.008
0.006
0.004
PROTONS/Mev cm² sec
10
100
1000
PARTICLE KINETIC ENERGY (Mev)

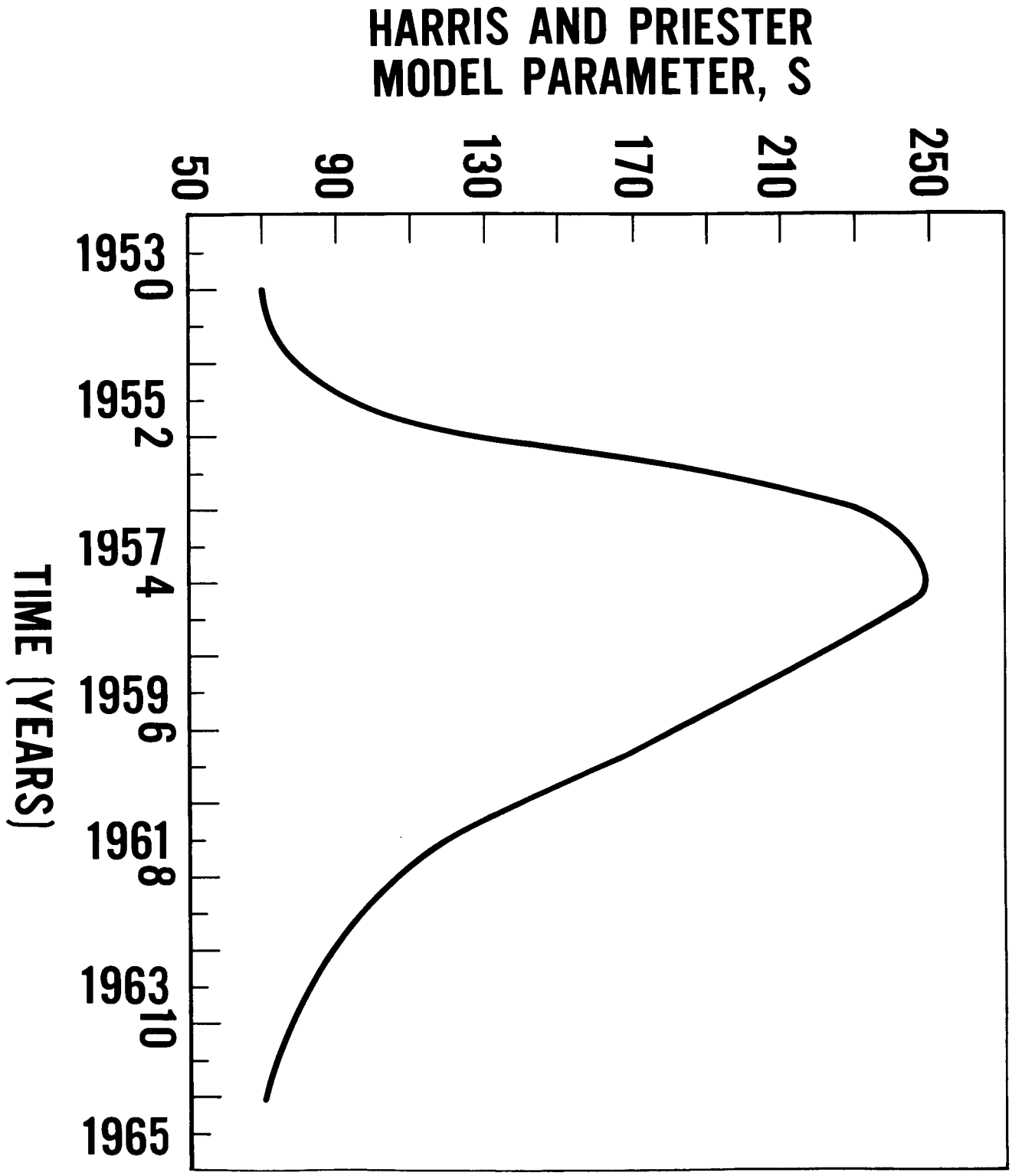
HARRIS AND PRIESTER
MODEL PARAMETER, S
50
90
130
170
210
250
TIME (YEARS)
1953
0
1955
2
1957
4
1959
6
1961
8
1963
10
1965

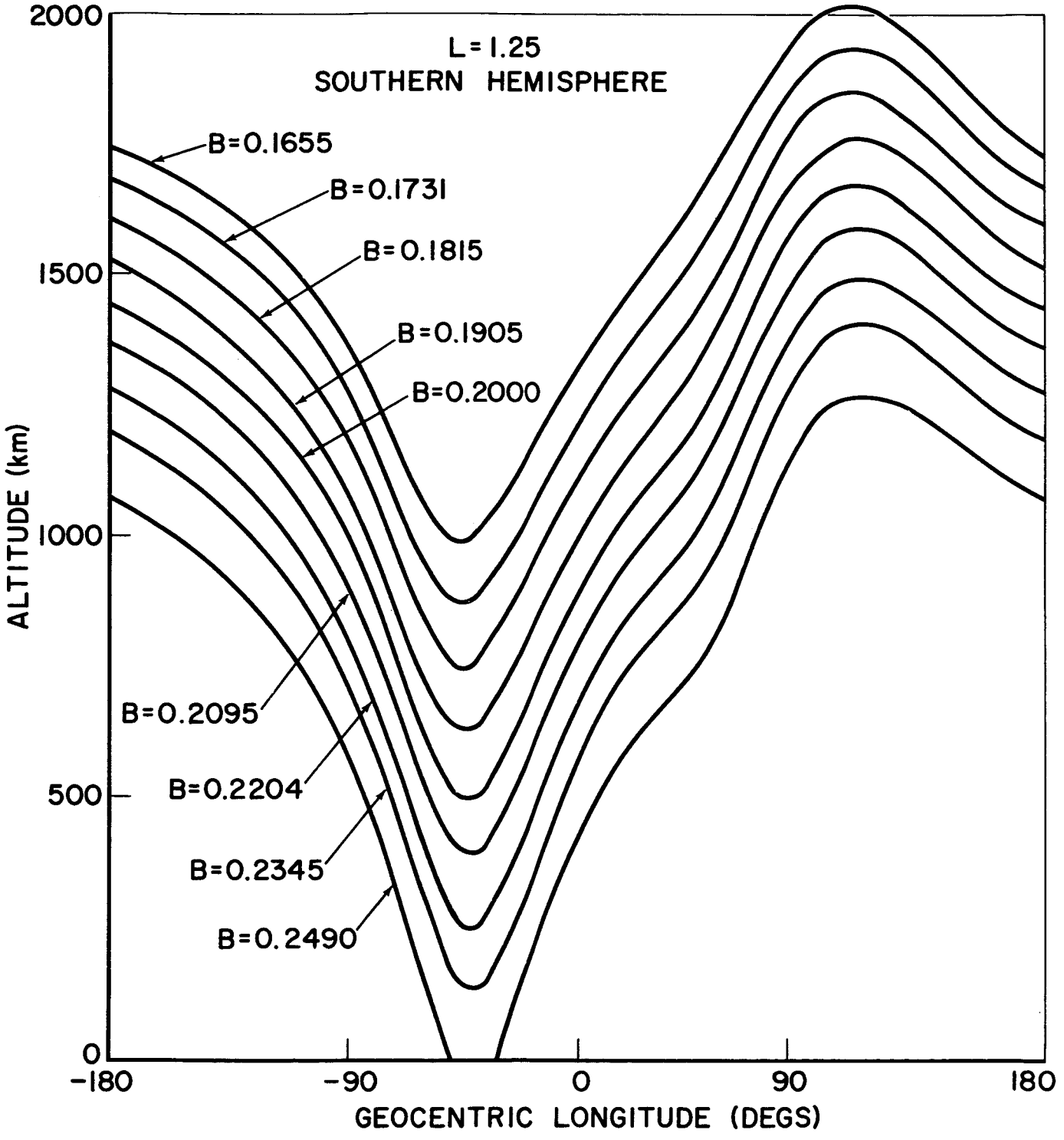
L = 1.25
SOUTHERN HEMISPHERE
B=0.1655
B=0.1731
B=0.1815
B=0.1905
B=0.2000
B=0.2095
B=0.2204
B=0.2345
B=0.2490
2000
1500
1000
500
0
ALTITUDE (km)
-180
-90
0
90
180
GEOCENTRIC LONGITUDE (DEGS)

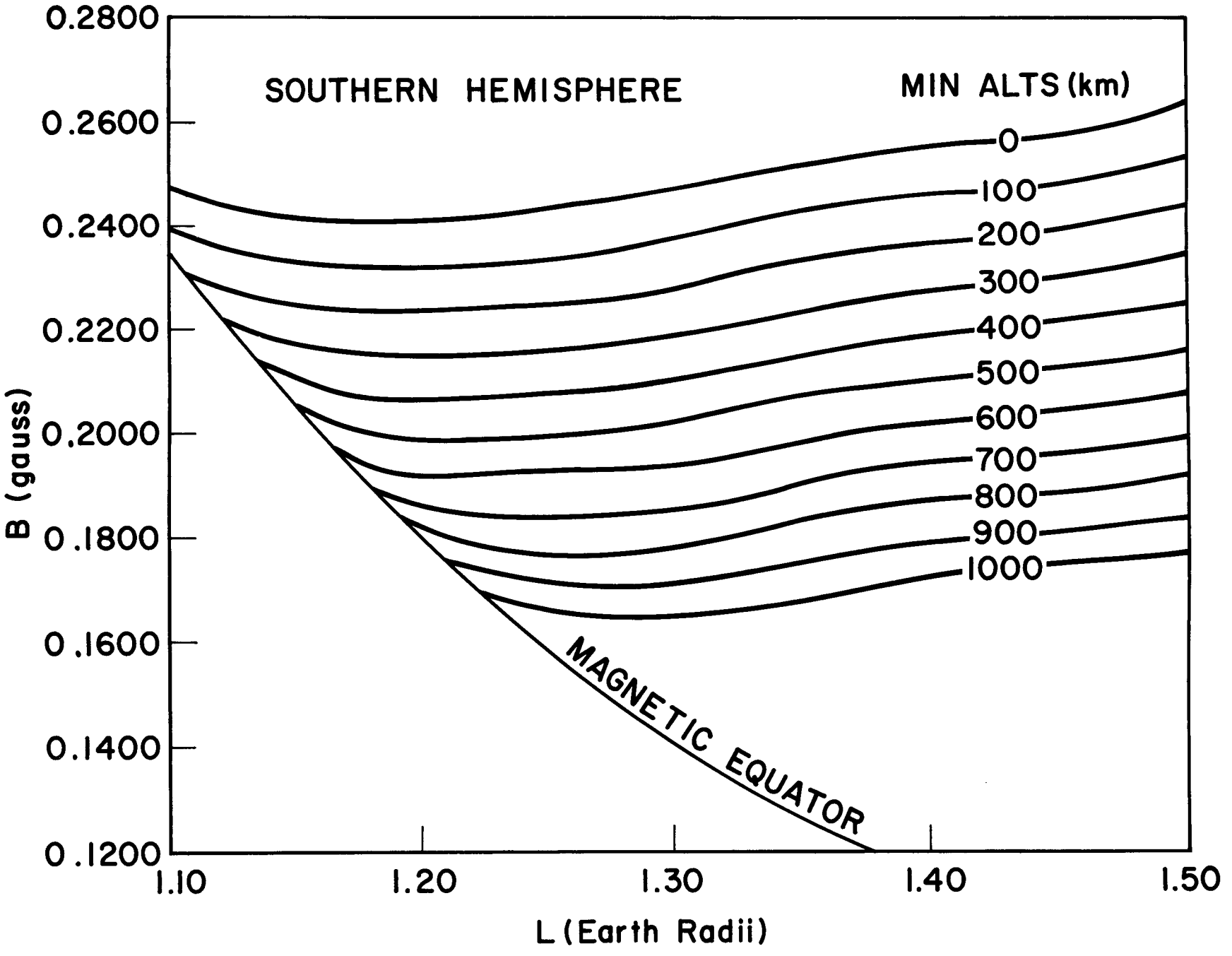
SOUTHERN HEMISPHERE
MIN ALTS (km)
0
100
200
300
400
500
600
700
800
900
1000
MAGNETIC EQUATOR
B (gauss)
0.2800
0.2600
0.2400
0.2200
0.2000
0.1800
0.1600
0.1400
0.1200
1.10
1.20
1.30
1.40
1.50
L (Earth Radii)

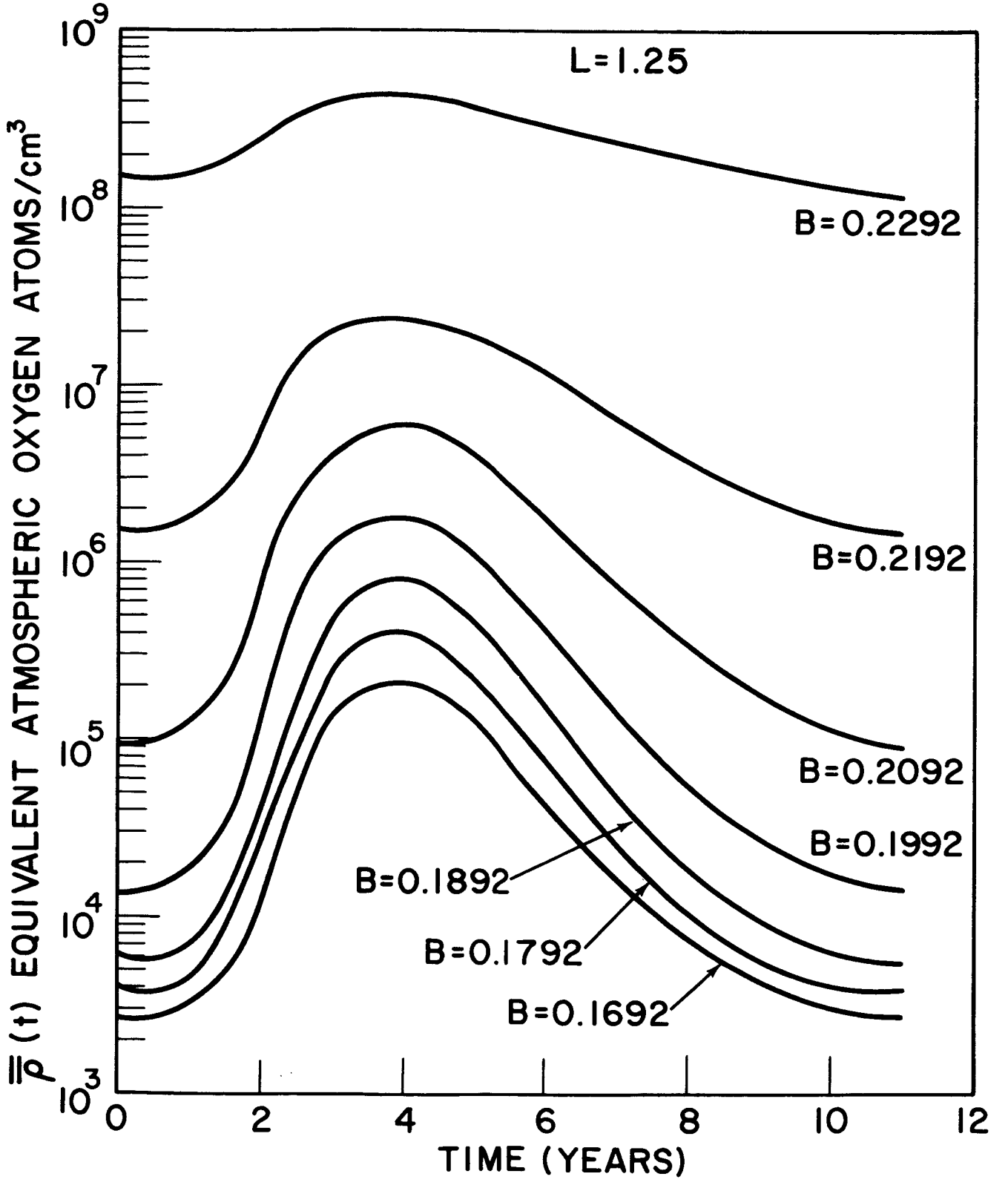
L=1.25
B=0.2292
B=0.2192
B=0.2092
B=0.1992
B=0.1892
B=0.1792
B=0.1692
$\bar{\rho}$ (t) EQUIVALENT ATMOSPHERIC OXYGEN ATOMS/cm^3
10^9
10^8
10^7
10^6
10^5
10^4
10^3
0
2
4
6
8
10
12
TIME (YEARS)

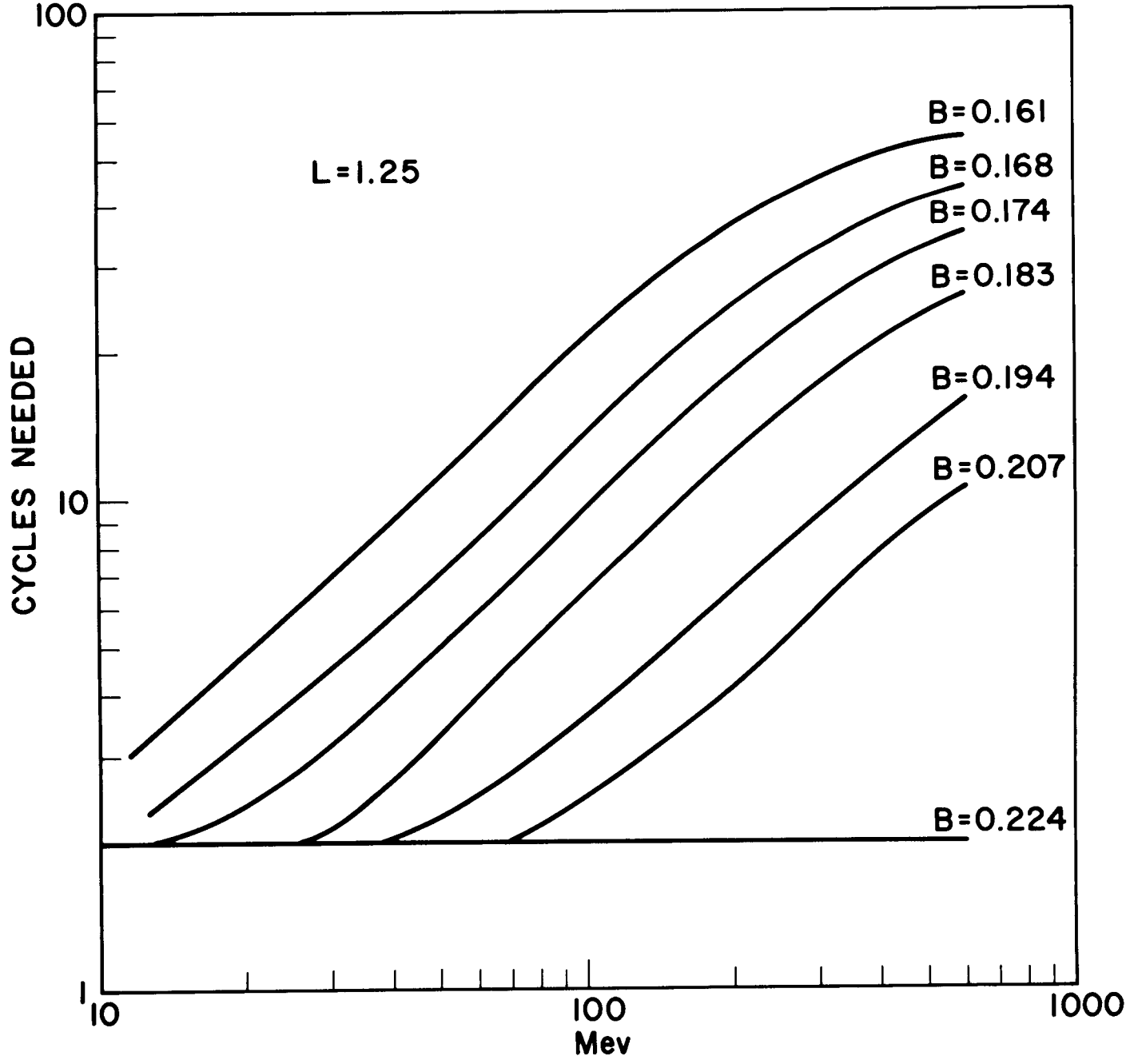
100
10
1
CYCLES NEEDED
L=1.25
B=0.161
B=0.168
B=0.174
B=0.183
B=0.194
B=0.207
B=0.224
10
100
1000
Mev

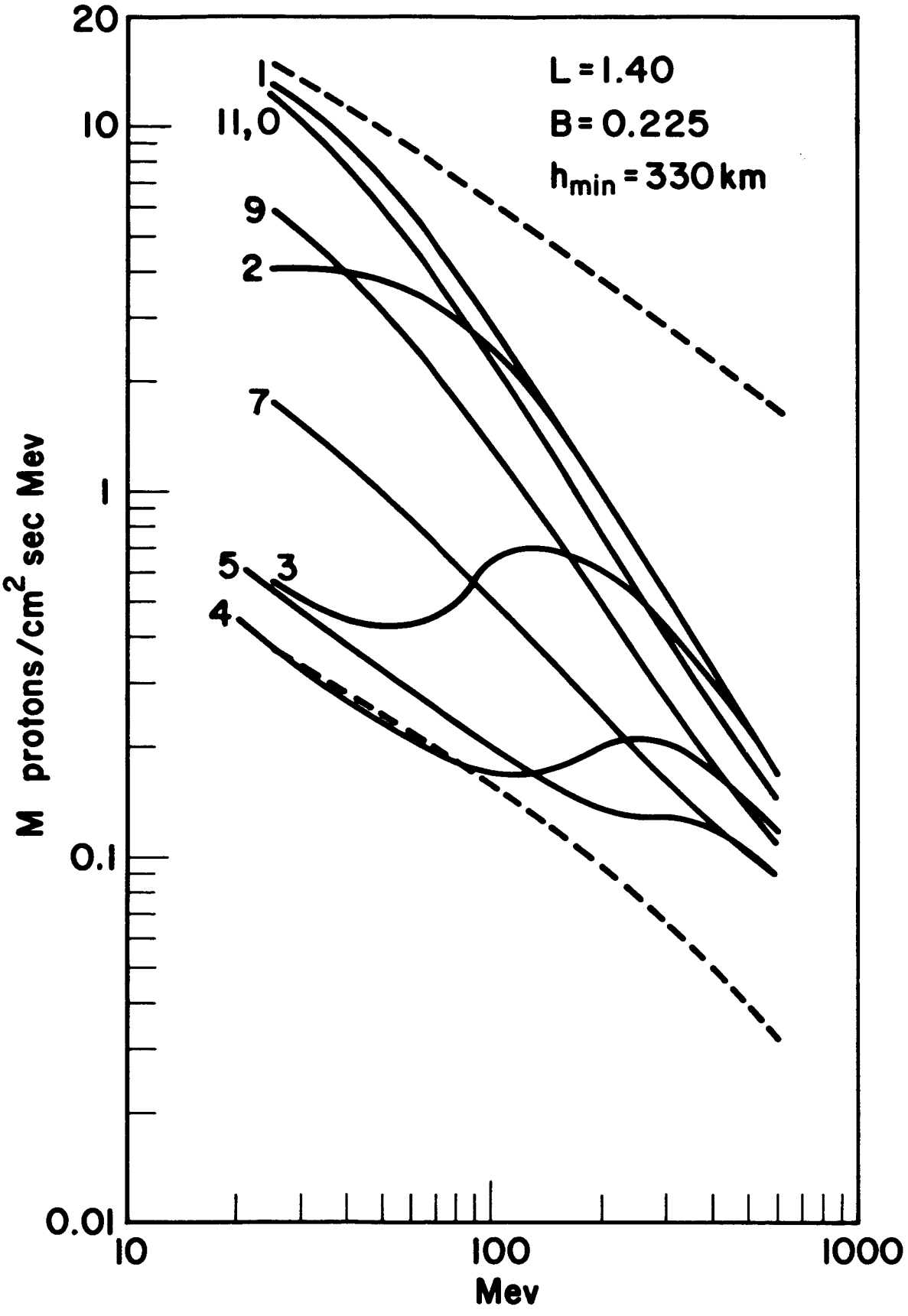
20
10
1
0.1
0.01
M protons/cm² sec Mev
L = 1.40
B = 0.225
h_min = 330 km
1
11,0
9
2
7
5
3
4
10
100
1000
Mev

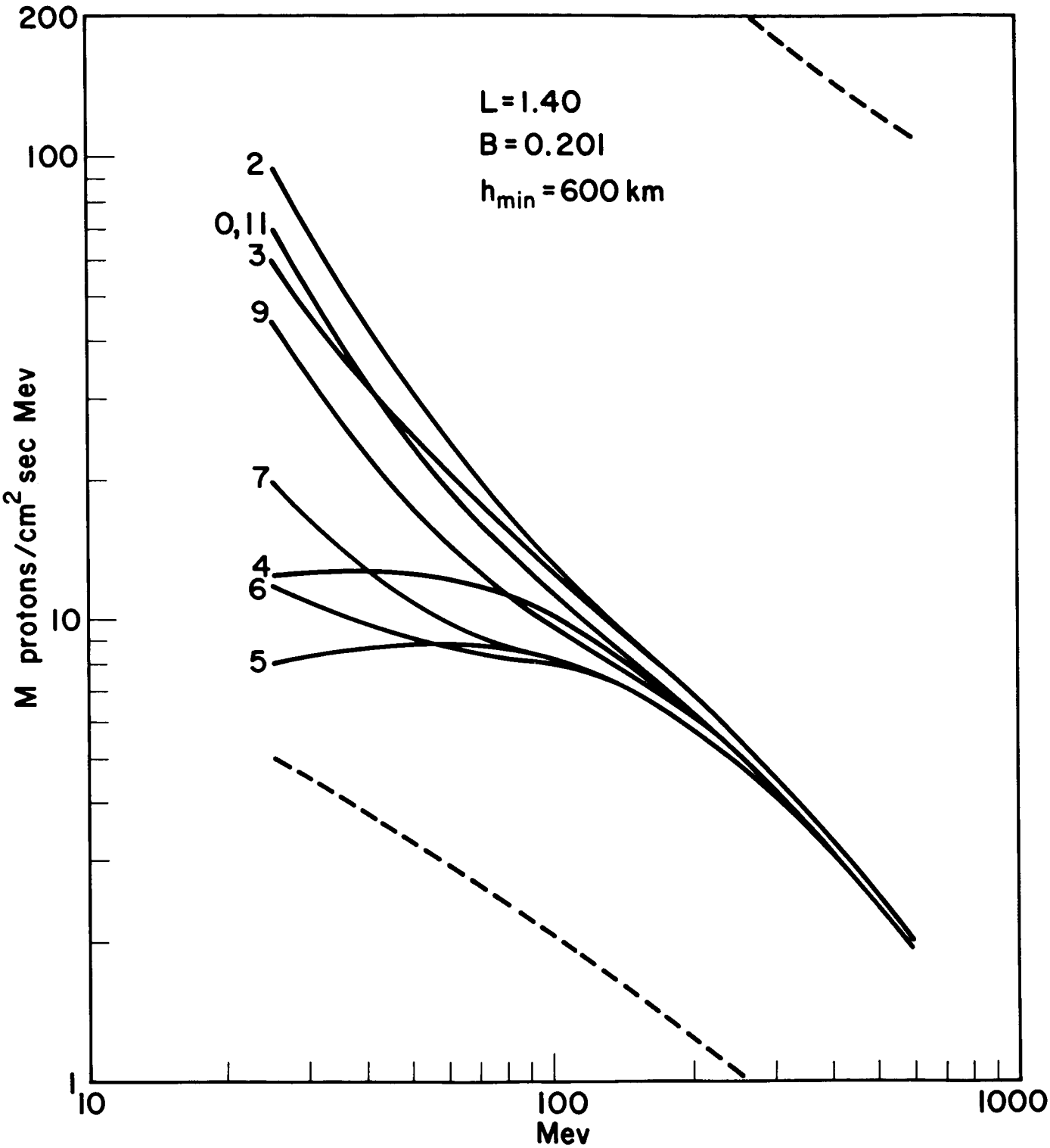
L=1.40
B=0.201
h_{min} = 600 km
2
0,11
3
9
7
4
6
5
200
100
10
1
M protons/cm^2 sec Mev
10
100
1000
Mev

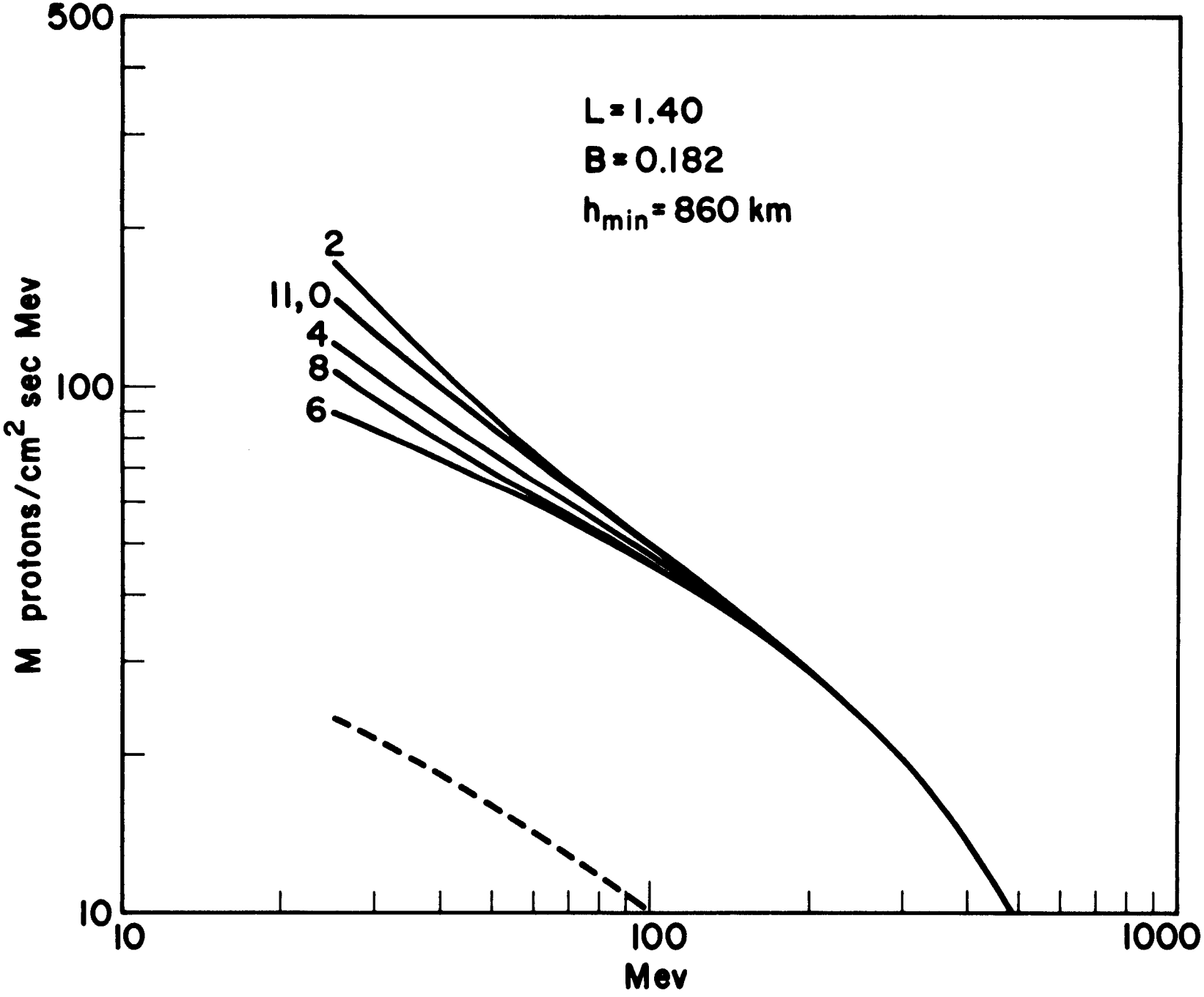
500
100
10
L = 1.40
B = 0.182
h_{min} = 860 km
2
11,0
4
8
6
M protons/cm^2 sec Mev
10
100
1000
Mev

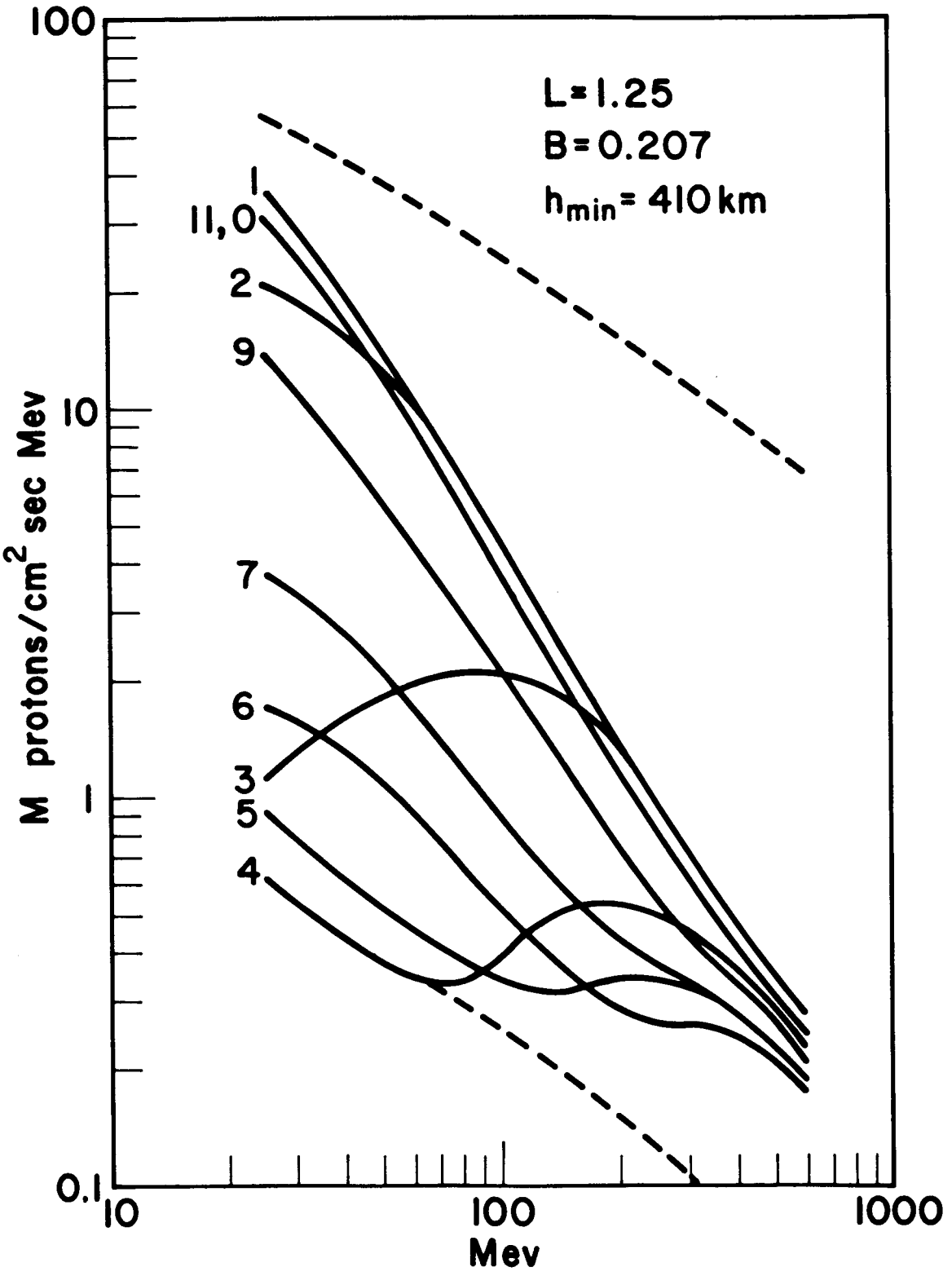
100
10
1
0.1
M protons/cm² sec Mev
L=1.25
B=0.207
h_min= 410 km
1
11,0
2
9
7
6
3
5
4
10
100
1000
Mev

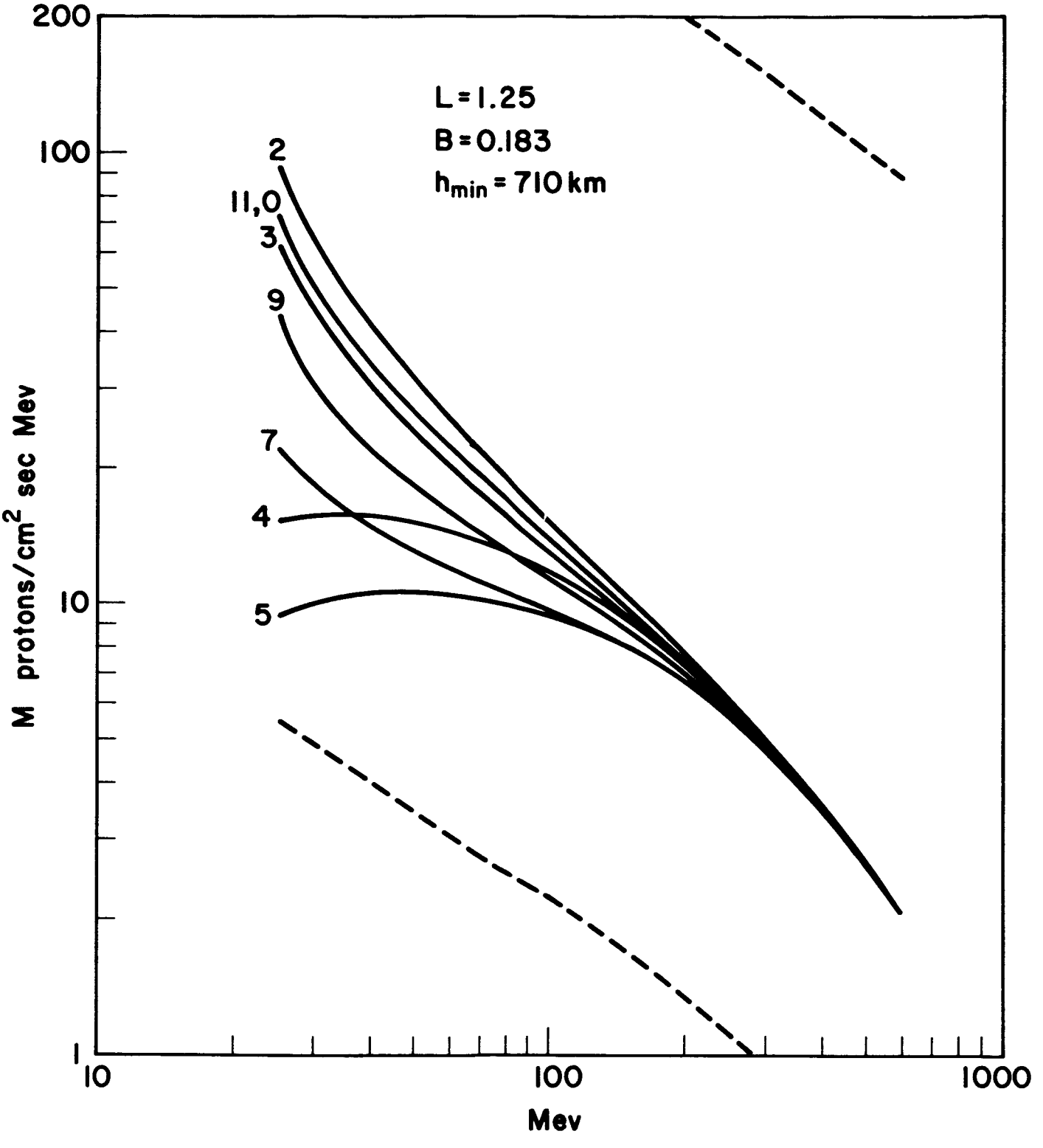
L = 1.25
B = 0.183
h_{min} = 710 km
2
11,0
3
9
7
4
5
200
100
10
1
10
100
1000
M protons/cm^2 sec Mev
Mev

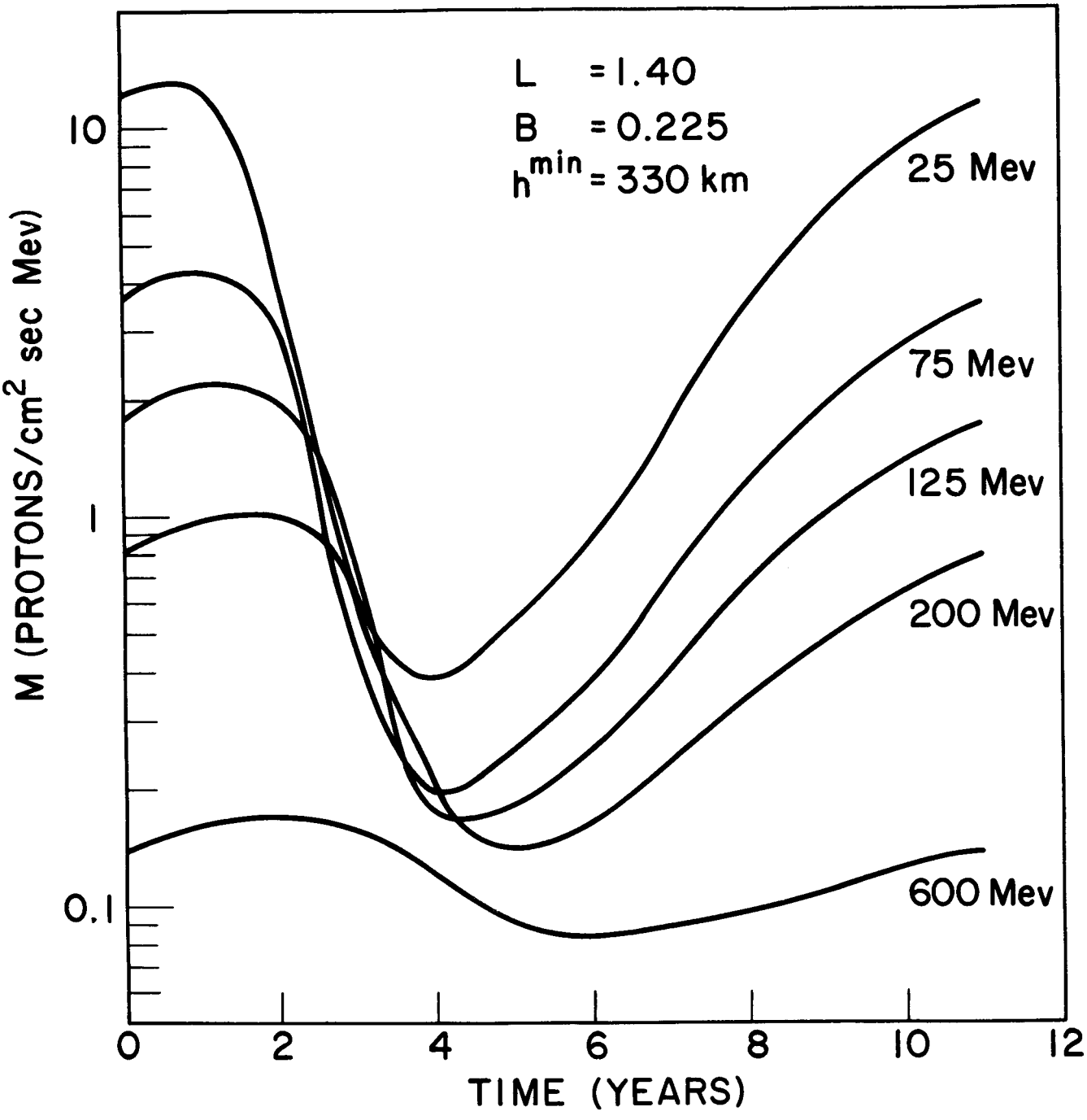
L = 1.40
B = 0.225
h^min = 330 km
25 Mev
75 Mev
125 Mev
200 Mev
600 Mev
10
1
0.1
M (PROTONS/cm² sec Mev)
0
2
4
6
8
10
12
TIME (YEARS)

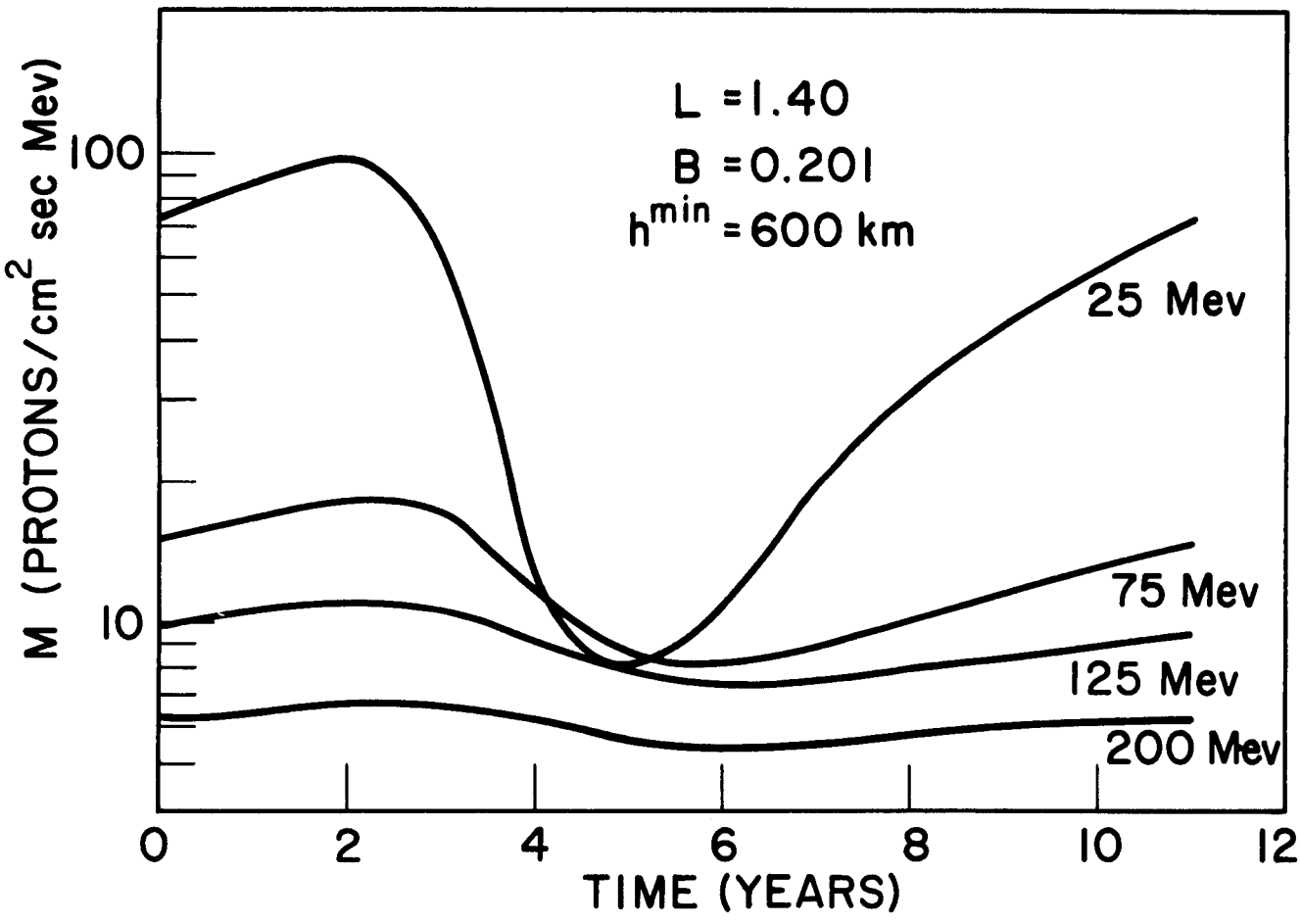
L = 1.40
B = 0.201
h^min = 600 km
25 Mev
75 Mev
125 Mev
200 Mev
M (PROTONS/cm² sec Mev)
100
10
0
2
4
6
8
10
12
TIME (YEARS)

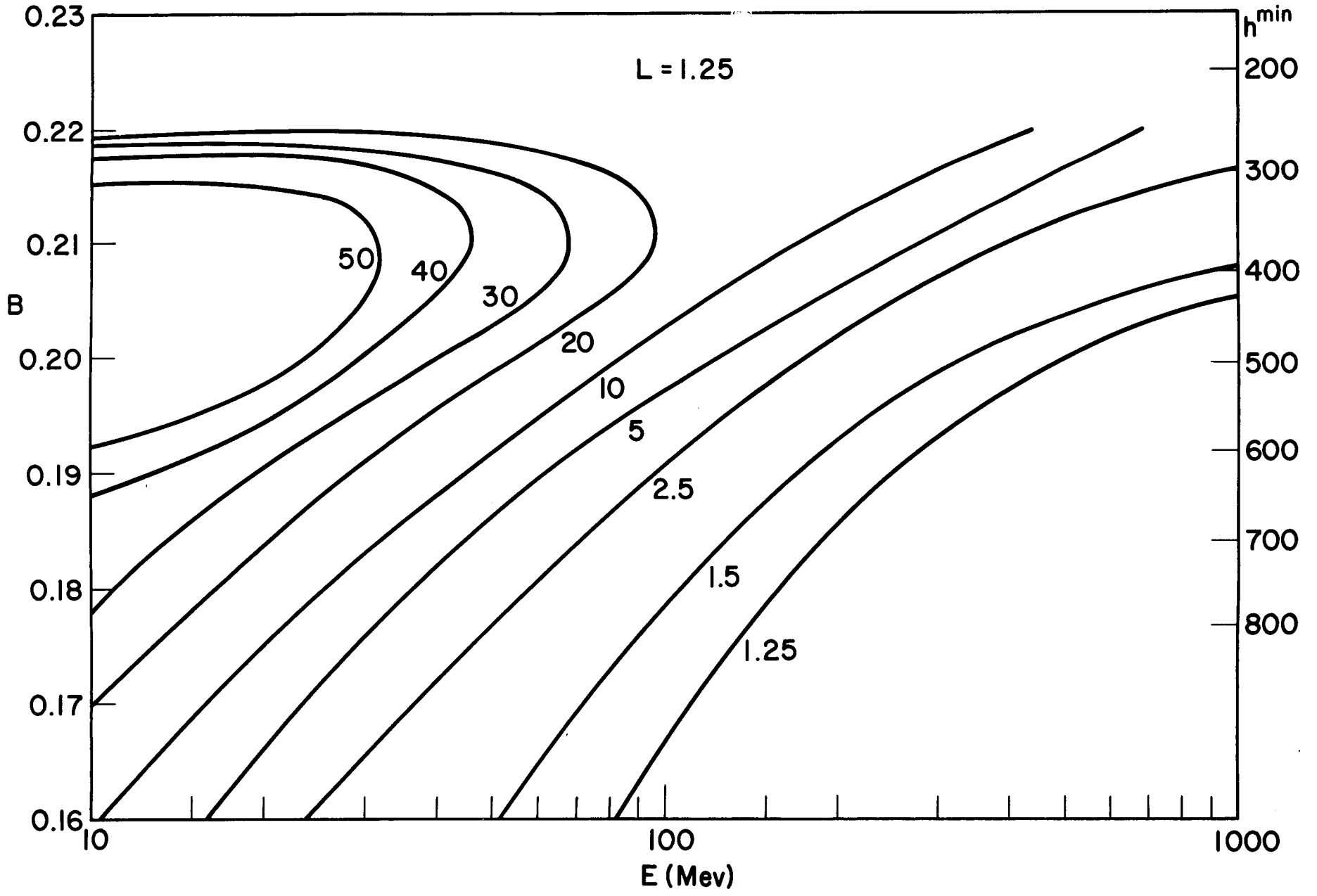
L = 1.25
B
0.23
0.22
0.21
0.20
0.19
0.18
0.17
0.16
50
40
30
20
10
5
2.5
1.5
1.25
h min
200
300
400
500
600
700
800
10
100
1000
E (Mev)

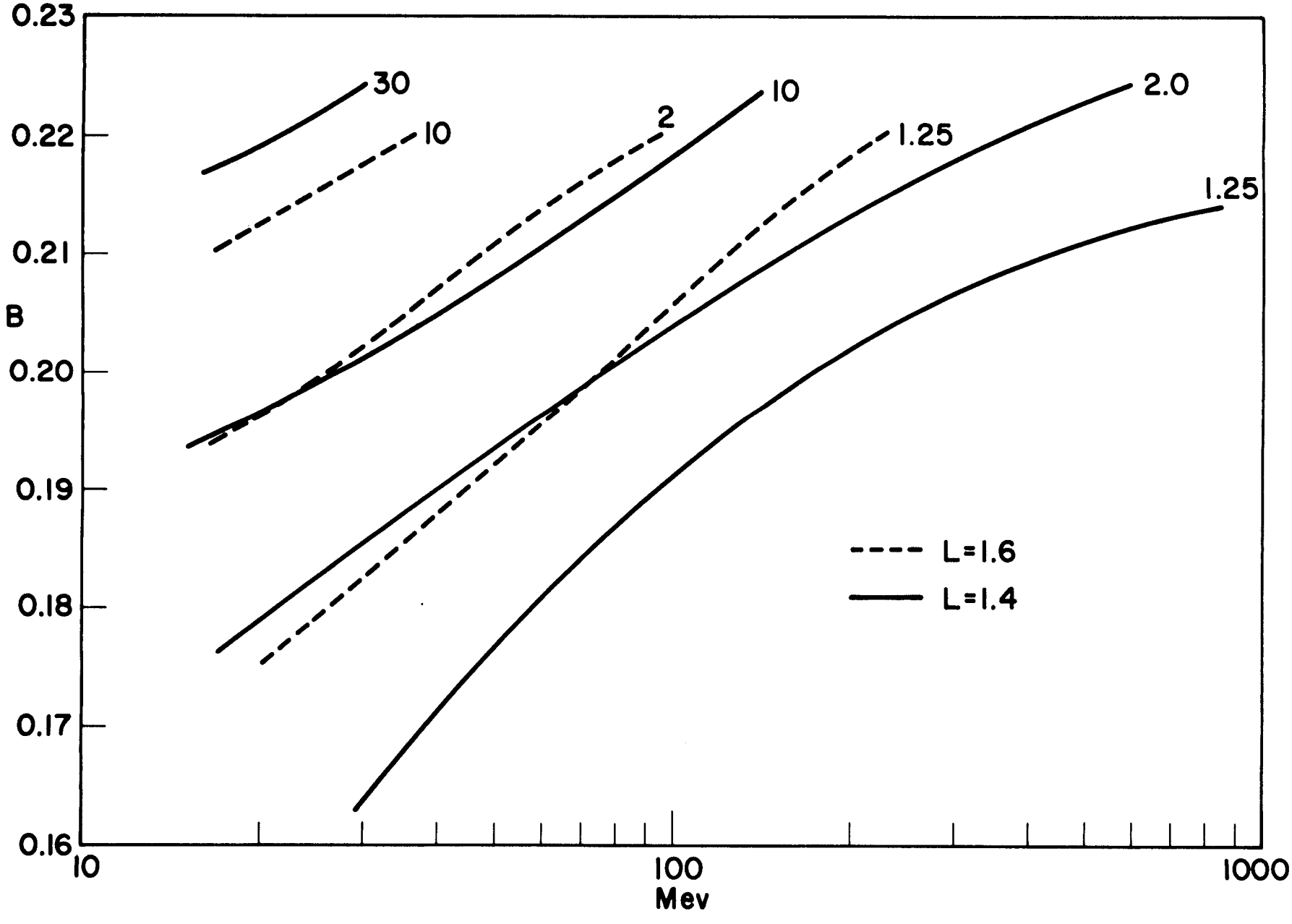
0.23
0.22
0.21
0.20
0.19
0.18
0.17
0.16
B
10
100
1000
Mev
30
10
2
10
1.25
2.0
1.25
L=1.6
L=1.4

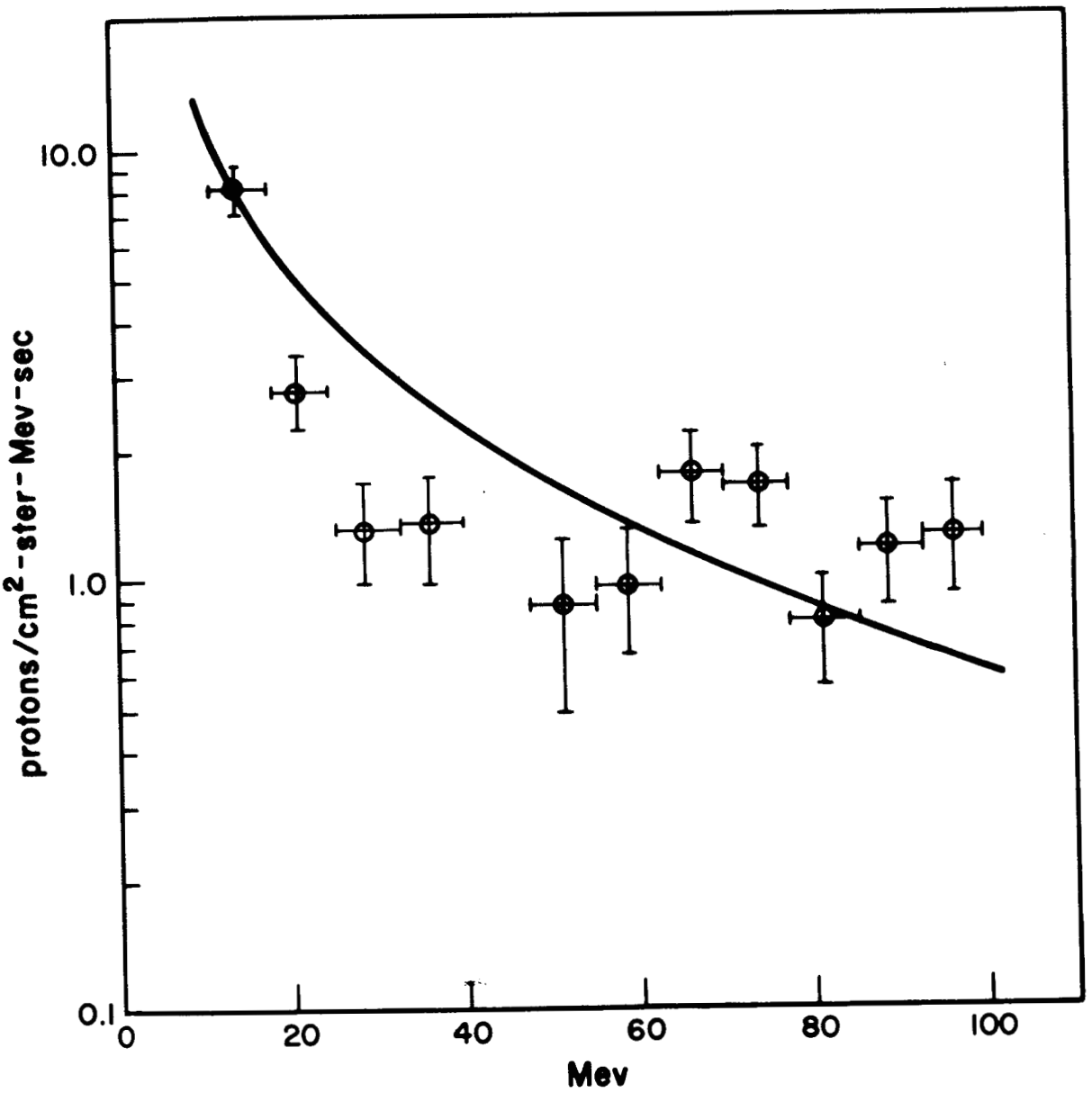
10.0
1.0
0.1
protons/cm²-ster-Mev-sec
0
20
40
60
80
100
Mev

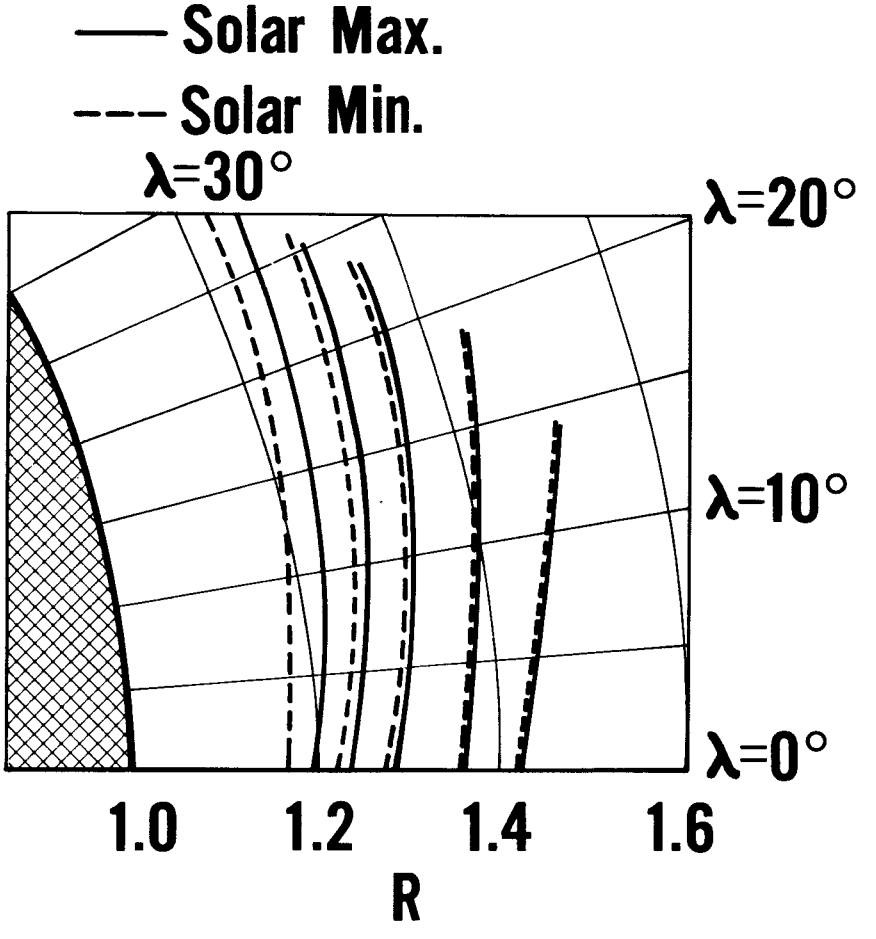
Solar Max.
Solar Min.
λ=30°
λ=20°
λ=10°
λ=0°
1.0
1.2
1.4
1.6
R

EXPERIMENT	DATE OF EXPERIMENT	TIME IN SOLAR ANGLE	L	B	H Min.	RESULTS OF EXPERIMENT	PREDICTIONS FROM PRESENT PAPER
(a) Naugle and Kniffen (1963)--Emulsions on NERV	Sept., 1960	6.7	(a) 1.54	.209	610 km	Spectrum ~ flat from 20 to 60 MeV $\frac{J_o\ (31)\ \text{at}\ 6.7}{J_o\ (31)\ \text{at}\ 4.1\ (\text{Exp. IV})} \sim k$	Spectrum should fall about a factor of 3 in this energy range (Fig. 8, curve 7) $\frac{J_o\ (31)\ \text{at}\ 6.7}{J_o\ (31)\ \text{at}\ 4} = 1.3$ (Fig. 8)
			(b) 1.47	.223	400 km	Spectrum ~ flat from 20 to 100 MeV $\frac{J_o\ (31)\ \text{at}\ 6.7}{J_o\ (31)\ \text{at}\ 4.1\ (\text{Exp. IV})} \sim 2.5$	Spectrum should fall about a factor of 4 in this energy range (Fig. 7, curve 7) $\frac{J_o\ (31)\ \text{at}\ 6.7}{J_o\ (31)\ \text{at}\ 4} = 3.5$ (Fig. 7)
(b) Freden and White (1962)--Emulsions on Atlas	1960	6.5	~ 1.40	~ .202	600 km	Spectrum peaks at ~ 40 MeV $\frac{J_o\ (20)}{J_o\ (40)} \sim .75$	No spectral peak at t = 6.5 (Fig. 8) $\frac{J_o\ (20)}{J_o\ (40)} \sim 2.0$ but at t = 5 do have spectral peak $\frac{J_o\ (20)}{J_o\ (40)} = 0.9$
(c) Pizzella, McIlwain and Van Allen--G M counter on Exp. VII	Oct. 1959 to Dec. 1960	5.8 to 7.0	1.40	.22	390 km	$\frac{J_o\ (E > 18)\ \text{at}\ 7.0}{J_o\ (E > 18)\ \text{at}\ 6.0} \sim 2.3$	$\frac{J_o\ (E = 25)\ \text{at}\ 7.0}{J_o\ (E = 25)\ \text{at}\ 6.0} = 2.0$ (Fig. 12)
(d) Filz and Yagoda--Emulsions on Discoverer	Dec. 1960 to June 1962	7.0 to 8.5	varying	varying	400 km	$\frac{J_o\ (E > 55)\ \text{at}\ 8.5}{J_o\ (E > 55)\ \text{at}\ 7.0} \sim 2.0$	$\frac{J_o\ (E = 75)\ \text{at}\ 8.5}{J_o\ (E = 75)\ \text{at}\ 7.0} \sim 2.3$ (Fig. 12)
(e) Heckman and Nakano--Emulsions on Low altitude polar satellites	Sept. 1962 to Sept. 1963	8.7 to 9.7	varying	varying	400 km	$\frac{J_o\ (65)\ \text{at}\ 9.5}{J_o\ (65)\ \text{at}\ 9.0} = 1.0 \pm .10$ $\frac{J_o\ (65)\ \text{at}\ 9.5}{J_o\ (65)\ \text{at}\ 4.1\ (\text{Exp. IV})} \sim 3$	$\frac{J_o\ (65)\ \text{at}\ 9.5}{J_o\ (65)\ \text{at}\ 9.0} = 1.2$ $\frac{J_o\ (65)\ \text{at}\ 9.5}{J_o\ (65)\ \text{at}\ 4.1} = 12$
(f) Freden and Paulikos--Solid state counters on Polar satellites	Sept. and Oct., 1962	8.8	1.30	.200	530 km	$\frac{J_o\ (7)}{J_o\ (85)} \sim 13$	
			1.47	.223	400 km	$\frac{J_o\ (7)}{J_o\ (85)} \sim 23$	$\frac{J_o\ (10)}{J_o\ (85)} \sim 11$ (Fig. 7)
			1.54	.209	610 km	$\frac{J_o\ (7)}{J_o\ (85)} \sim 43$	$\frac{J_o\ (10)}{J_o\ (85)} \sim 24$ (Fig. 8)
			low	high		$\frac{J\ (E > 31)\ \text{at}\ 8.8}{J\ (E > 31)\ \text{at}\ 4.1\ (\text{Exp. IV})} \sim 3$	$\frac{J\ (E = 50)\ \text{at}\ 8.8}{J\ (E = 50)\ \text{at}\ 4.1} = 13$
(g) Rowland Bakke, Imhof, Smith (1963) scintillators on Atlas pods	March, 1963	9.2	1.27	.216	340 km	no maximum at 40 MeV $\frac{J_o\ (20)}{J_o\ (40)} \sim 2.0$	$\frac{J_o\ (20)}{J_o\ (40)} = 2.2$ (Fig. 10)
						$\frac{J_o\ (10)}{J_o\ (60)} \sim 8.0$	$\frac{J_o\ (10)}{J_o\ (60)} = 9.0$